Austin Journal of Clinical Neurology

Open Access

Austin Publishing Group

Research Article

Early Detection of Amyloid Plaques in Mouse Models of Alzheimer's Disease by PET with ^{18}F-Hydroxy Quinoline

Kulkarni PV[1]*, Alhasan M[2], Chiguru S[1], Arora V[1], Slavine N[1], Hao G[1], Sun X[1], Antich P[1] and Bonte FJ[1]

[1]Department of Radiology, UT Southwestern Medical Center, Center at Dallas, TX, USA

[2]Department of Allied Medical Sciences, Jordan University of Science and Technology, Jordan

***Corresponding author:** Kulkarni PV, Department of Radiology, UT Southwestern Medical Center, 5323 Harry Hines Blvd., Dallas, TX, USA

Received: April 14, 2015; **Accepted:** June 16, 2015; **Published:** June 28, 2015

Abstract

Goal of the study was to evaluate ^{18}F-(8-hydroxy) quinoline (^{18}F-HOQ) by PET in transgenic (Tg) animal models of Alzheimer's disease (AD). Five groups of mice (n=4 per group) were used; control (WT, 12 mo), APP/PS Tg mice (4, 6, and 12 mo) and APOE4 Tg mice (12 mo). ^{18}F-HOQ was prepared as previously reported by us. Animals were imaged in a PET/CT scanner for 30 minutes immediately after intravenous injection of the tracer and SUV values for various brain regions determined. After imaging, animal brain sections were stained and amyloid plaque burden measured. Cortex, olfactory bulbs and hippocampus had higher activity compared to cerebellum and were significantly higher ($p<0.05$) in APP/PS1 Tg mice compared to WT or APOE4 mice. Only APP/PS1 mice brain sections were positive for Aβ. Tracer uptake by PET correlated with plaque density measured by histopathology. Plaque density increased with age. Differences in brain uptake by PET could be observed at an early age (4 mo) only in APP/PS1 mice. F-18 HOQ may be useful in monitoring the progression of Aβ plaque deposition in suitable AD animal models by PET and in assessing efficacy of therapeutic agents aimed at reduction of amyloid plaque burden.

Keywords: Alzheimer's disease; Transgenic animals; Plaques; PET/CT imaging

Introduction

Alzheimer's disease (AD) is the most common cause of dementia. AD is a neurodegenerative disorder of enormous socioeconomic burden [1]. It represents auto-inflammatory reaction resulting in the activation of the immune system in response to aberrant proteins located in the brain and leading to neurotoxicity [2]. Neurodegenerative disorders are defined as progressive loss of neurons. The pathologic hallmarks of AD are extracellular beta amyloid (Aβ) plaques and intracellular neurofibrillary tangles (NFTs) [3]. The amyloid cascade hypothesis has explained the mechanism of the disease based on the presence and the deposition of the amyloid plaques [4]. The abnormal function of these intracellular and extracellular proteins results in death of neurons [5]. Noninvasive detection of deposition of Aβ plaques is important in understanding the pathology of early AD. The development of radiopharmaceuticals for medical imaging with positron emission tomography (PET) may provide an ideal non-invasive methodology to enable early diagnosis, monitor disease progression, differential diagnosis, and evaluate drug therapies of patients with AD and related dementias [6-8]. A number of recent articles have reviewed the progress in development of imaging agents targeting beta amyloid [9-13].

A number of molecules including derivatives of Thioflavin and Congo red, labeled with carbon-11 (^{11}C; $t_{1/2}$ = 20.4 min) and fluorine-18 (^{18}F; $t_{½}$ = 109.7 min) have been synthesized and investigated for imaging amyloid plaques and tangles with promising results [14-18]. Fluorine-18 labeled agents are more desirable than those labeled with carbon-11 because of relatively longer half-life affording longer radio-synthesis, imaging protocols and option for supply by a commercial manufacturer to imaging sites without a cyclotron and/or radiochemistry laboratories. Majority of radiotracers for imaging AD are based on Congo red or thioflavin derivatives with affinity for amyloid Aβ plaque deposits. The most widely used radiotracer for imaging AD is a labeled thioflavin analog, *N*-methyl-[^{11}C]2-(4'-methylaminophenyl)-6-hydroxybenzothiazole (referred to as Pittsburgh Compound B or PiB), [15, 17] with recent efforts directed towards labeled styrylpyridine and stilbene derivatives [18].

Among the transitional elements iron, zinc and copper are essential to human health. However they also have shown to be involved in AD. Copper overload has been associated with mental decline [19] and particularly AD development [20, 21]. As the most abundant trace metal in the brain, zinc is tightly associated with numerous proteins. Role of zinc and copper in neurodegenerative process have been extensively reviewed [22, 23]. Deposition of amyloid plaque protein is intimately associated with the increased levels of transition metal ions such as Cu^{2+} and Zn^{2+} [24-30]. High concentration of zinc (up to 1 mM) have been found within amyloid plaques [24], which is thought to have been released from glutamatergic synapses [25]. Hydroxyquinoline (HOQ) and its derivatives are under investigation for therapeutic applications based on extraction of metal ions and disaggregation of plaque [31-38]. Kinetically slow re-extraction of Zn could be useful potentially in imaging amyloid plaque using transition metal chelating agents. Opazo et al utilized this strategy in exploring radio iodinated clioquinol (CQ) as a biomarker for β–amyloid in human subjects [39]. Using autoradiography imaging, ^{125}I-CQ was demonstrated to be specific for imaging β–amyloid plaque in histological samples. However, a large portion of administered ^{123}I-CQ was taken up by liver and metabolized and less than 1% of this activity was taken up by brain. Further, it can undergo facile de–iodination *in vivo*. Thus, [^{123}/^{124}I] CQ might not be ideal for diagnostic

Citation: Kulkarni PV, Alhasan M, Chiguru S, Arora V, Slavine N, Hao G, et al. Early Detection of Amyloid Plaques in Mouse Models of Alzheimer's Disease by PET with ^{18}F-Hydroxy Quinoline. Austin J Clin Neurol 2015;2(8): 1065.

imaging of AD. We designed polybutylcyanoacrylate nanoparticles with incorporated radio ligands and amyloid affinity agents that are attracted to Aβ protein. We evaluated nanoparticulate radio labeled quinolone to detect amyloid plaques in mouse models of AD [40].

A small, blood brain barrier (BBB) permeating, stable and non–polar ^{18}F labeled HOQ that forms a rapid and reversible ternary complex with Zn–Aβ fibrils could be useful for imaging amyloid plaques with high specificity. Previously we reported the synthesis of ^{18}F–2–fluoro–8–hydroxy quinoline (^{18}F-HOQ) and preliminary evaluation in imaging of AD plaques in APP/PS1 transgenic mice [41, 42]. Here we report the evaluation the tracer in PET imaging of APP/PS1 and APOE4 transgenic mice of different ages, also assessed the possibility of analyzing the regional tracer uptake and washout kinetics in mice brain similar to other plaque imaging agents in human brain. Uptake of tracer in mice brain was measured by PET/CT imaging and correlated with the amyloid burden by histology.

Although current transgenic (Tg) animal models obviously do not manifest all clinical and pathological aspects of AD, nonetheless they are useful in testing of novel intervention strategies and imaging agents.

Methods

Animal models

There are number of animal models of AD and may not truly represent the human AD. However, they are valuable tools in evaluating experimental imaging and therapeutic agents. The animal experimental protocol was reviewed and approved by the Institutional Animal Care and Use Committee (IACUC) of UT Southwestern Medical Center. Here in our study we used double (APP/PS1) double transgenic and APOE4 transgenic mice in evaluating fluorine-18 labeled quinolone. Double transgenic mice with double mutation (APP/PS1) for Alzheimer's disease were used (Strain: B6C3–Tg) (APPswe, PSEN1dE9)85Dbo/J). This particular model corresponds to a form of early onset of disease and expresses mutant human presenalin 1 (DeltaE9) and a chimeric mouse/human amyloid precursor protein (APPswe) and APOE4 Tg mice representing late onset of AD [43-45]. APP transgenic mice were obtained from Dr. Qu laboratory at UT Southwestern and have been well characterized by gene typing [46].Three groups of mice (n=4 per group) were used for PET imaging studies: 1. control (WT), 2. Tg mice, APP/PS1, (strain B6C3-Tg, APPswe, PSEN1 dE9) and 3. APOE4 Tg mice (Taconic, #1549, C57BL/6), ages 11-12 months. Frozen brain sections of APP/PS1 Tg and control (WT) mice were incubated with ^{18}F-HOQ (50μCi/mL), washed and exposed to Phosphor Imaging Plate® for 2 h and images quantified as digital light units (DLU). Autoradiography, histology and *in vitro* studies were reported in details somewhere else [42].

Small animal PET/CT imaging

Small animal PET/CT imaging studies were performed using a Siemens Inveon® Micro PET/CT system (Siemens Medical Solutions Inc., Knoxville, TN, USA). Ten minutes prior to imaging, the animals were anesthetized using 3% Isoflurane at room temperature until stable vital signs were established. Once the animal was sedated, the animal was placed onto the imaging bed under 2% Isoflurane anesthesia for the duration of the imaging. The micro CT imaging was acquired at 80kV and 500 μA with a focal spot of 58μm. The PET images were acquired directly following the acquisition of CT data. Radiotracer (50-90 μCi) was injected intravenously via the tail vein. Immediately following the injection, a 20-30 minute dynamic scan was performed. PET images were reconstructed using Fourier Rebinning and Ordered Subsets Expectation Maximization 3D algorithm with dynamic framing every 60 seconds. Reconstructed images were fused and analyzed using Inveon® Research Workplace (IRW) software.

F-18 quinoline (^{18}F-HOQ) was prepared as previously reported by us; reacting 8-benzyloxy-2-chloroquinoline with K222 and F-18 in DMSO and purified by HPLC [5, 6]. Tg AD and WT mice (n=4 per group), were scanned in a Siemens Inveon® PET/CT scanner for 30 minutes immediately following i.v. injection. SUV values for various brain regions were determined using AMIDE® software and an MRI 3D mouse brain atlas. After imaging studies, animal brains were taken out, fixed and brain tissue sections were stained with an antibody specific to Aβ and plaque burden measured with Image J ® software.

PET/CT analysis using MRI brain atlas

PET/CT images analyzed using AMIDE software and a 3D mouse brain atlas. PET images (voxel volume: 0.9×0.9×0.8 mm) were overlaid on the CT images (voxel volume: 0.2×0.2×0.2 mm). The registration of the images was performed by identifying three anatomical regions (e.g. heart, kidneys and the brain) on both images. The brain region was segmented based on a 3D mouse brain atlas (voxel volume: 0.06×0.06×0.06 mm) into distinct areas where the plaques are mostly found.

These areas include olfactory bulb, cerebral cortex, hippocampus and to lesser extent cerebellum [14-18]. 3D ROIs were selected to cover these regions in each plane including axial, coronal and sagittal plane (Figure 1). The activity in each region was quantified using standardized uptake value (SUV):

SUV = % ID/g tissue × Ws ÷ 100

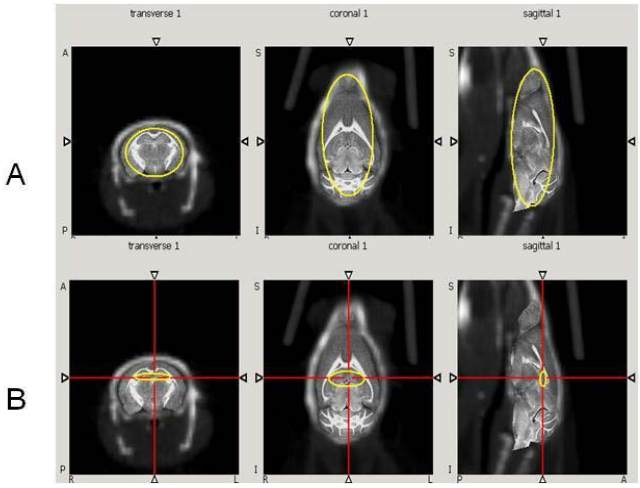

Figure 1: CT/MR mouse brain atlas registration. The first row (A) shows the 3D ROI of total brain region. The second row (B) shows the 3D ROI of hippocampus region. Both regions were selected on the transverse, coronal and sagittal planes respectively.

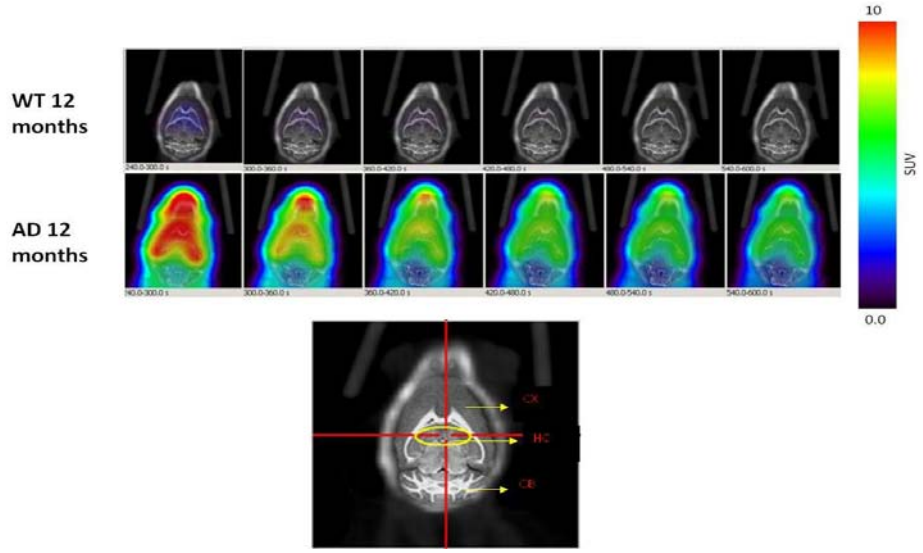

Figure 2: Dynamic PET images (1 min/image, 5min-10min) post injection of ^{18}F-HOQshow the differences between brain uptake in 12 months old control (1st row) and AD mice (2nd row). The view is coronal section at the level of the hippocampus as indicated in the brain atlas labeled image.

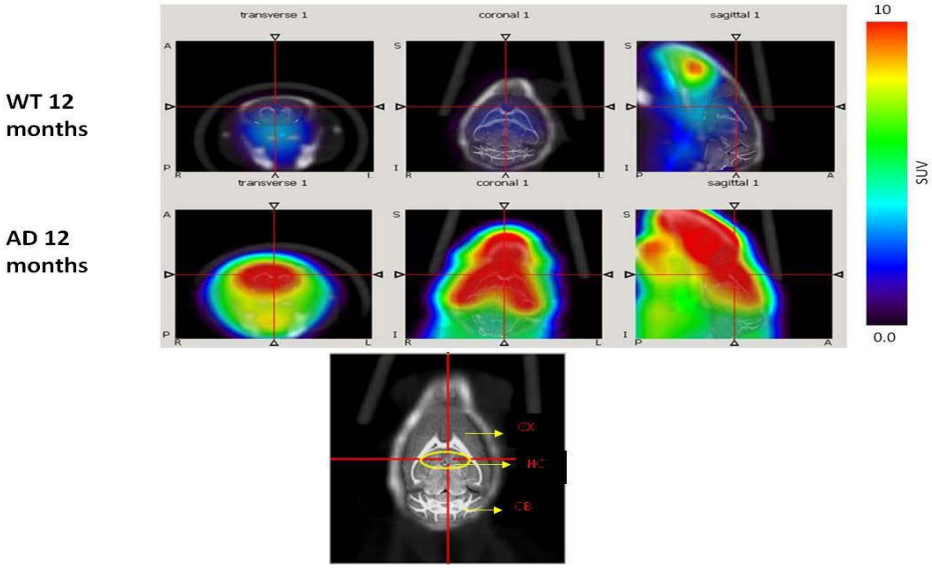

Figure 3: PET images (cumulative images 5min-10min post injection of ^{18}F-HOQ) show the differences between brain uptake in 12 months old control (1st row) and AD (2nd row) mice. The view is coronal section at the level of the hippocampus as indicated in the brain atlas labeled image.

Where ID is the injected dose, Ws is the subject weight [19]. Time activity curves (TACs) of the brain region were fitted into two phase exponential decay equation to calculate the decay parameters using MATLAB software.

$a * \exp(-b * x) + c * \exp(-d * x)$

b, fast rate constant, fast half-life (0.693/b)

d, slow rate constant, slow half-life (0.693/d), a and c are coefficients

Statistical analysis

SUV values were normalized to the first time point and area under curve (AUC) of the TACs was calculated for AD and control mice. *Student's t-test (p=0.05: significant level)* was used to compare control group to AD group generated by Graph Pad Prism® software.

An Iterative Deconvolution Method for Fast Quantitative Image Recovery

A rapidly converging, iterative deconvolution algorithm with a novel resolution subsets-based approach (RSEMD) [47] to de-noise and improve the quality of PET images is used. The RSEMD iterates the blurred image with different resolution parameters (to maximize SNR) and a corresponding number of iterations for each resolution subset (intermediate image after one or more iterations) are taken in turn. In this case the total number of iterations after all of the resolution subsets are employed is much less compared

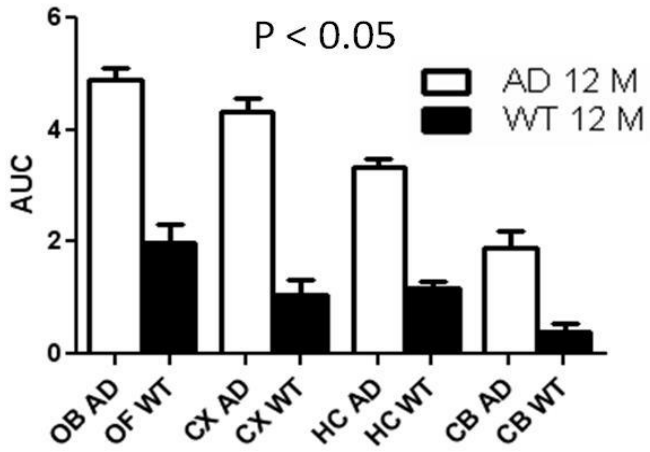

Figure 4: Area under the curve (AUC) of TACs for different regions of mice brains). Data represent average AUC ± SE. *Student's t-test showed significant difference (P<0.05) at different regions. (OB=Olfactory bulb, CX=Cortex, HC=Hippocampus, CB=Cerebellum, WT= Wild type).*

to other methods which use one resolution parameter for multiple image updates passed through the data. The reconstruction time with RSEMD is improved by a factor of 4-5 compared to other iterative reconstruction methods.

Results

Dynamic (1 min/image) PET images (5-10 min. post injection) showed that the tracer washout from AD mice brains was slower compared to control mice as can be seen qualitatively (Figure 2). Sum images (5-10 minutes post injection) showed higher retention of the tracer in AD mice brains compared to control mice brains (Figure 3). Area under curve of TACs of AD mice (n=4:12 months) showed more retention of the activity over 10 min in comparison to the control mice (n=3: 12 months) for different regions of the brain including olfactory bulb, cerebral cortex, hippocampus and cerebellum (Figure 4). There was a significant difference between AD and control mice (*P<0.05)* in terms of AUC of different regions. Data are expressed as SUV (specific uptake value) normalized to the first time point. During the first 2 min, there was a rapid clearance of the compound in both (control and AD) mice. However, AD mice brains had slower clearance than the control mice. The retention time of the tracer was higher for the AD mice in both decay phases (Figure 5).

The regional analysis of the PET images demonstrated higher uptake in the regions associated with the plaques. In addition, cerebral regions have more activity than the cerebellum. Dynamic PET images demonstrated fast clearance of the compound in the normal brain and higher accumulation in the cerebral regions of the AD mice than the cerebellum region (Figure 6). Integrated activity (0-600s) showed more retention of the compound in the AD mice brains in comparison to control mice (Figure 6).

Autoradiography images showed higher uptake for AD brain sections in comparison to control. In addition, regional analysis for autoradiography demonstrated higher activity for the cortex and the cerebellum of AD in comparison to control mice. The results reflect similar pattern as observed in the PET imaging (Figure 6). Immunohistochemistry results showed variation in the plaques

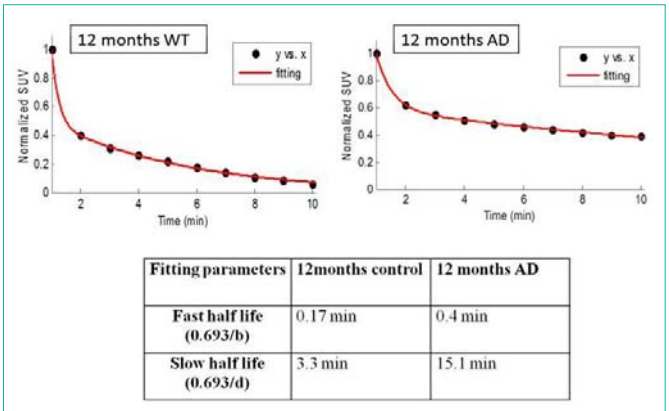

Fitting parameters	12months control	12 months AD
Fast half life (0.693/b)	0.17 min	0.4 min
Slow half life (0.693/d)	3.3 min	15.1 min

Figure 5: Time activity curves (TACs) fitting for total brain region. Half-life of the compound in both decay phases was shorter in control than in AD mice indicating longer retention of the tracer in AD mice.

density in different regions of AD brain including cerebral cortex, hippocampus and the cerebellum. PET imaging showed higher uptake, and histology showed higher plaque density in the cerebral cortex than the cerebellum (Figure 7).

^{18}F-HOQ showed high binding affinity for Aβ-Zn aggregates (Kd=1.5 nM)(data not shown). Autoradiographic data (digital light unit, DLU) correlated with plaque density (Figures 6 and 7). Integrated brain activity over 10 min for cortex, olfactory bulbs and hippocampus had higher values compared to cerebellum and were higher ($p<0.05$) in APP/PS1 Tg mice compared to WT mice (Figure 6). There was no difference between APOE4 and control mice. The values increased with age in APP/PS1 AD transgenic mice and correlated to plaque density [R^2=0.88] (Figure 7 and 8).

Discussion

Hydroxy quinoline derivatives are weak chelating agents. They bind to transition metals such as zinc, copper and iron without resulting in metal depletion [39-42]. Among biologically relevant metals in the brain, zinc was found to be the most elevated metal in the AD brain mostly in the hippocampus and the cerebral cortex [24,39]. This supports the imaging results where the compound retention was higher in the cerebral regions in comparison to the cerebellum. In addition, normal brain showed some activity retention especially in hippocampus and the cortical regions. This finding could be related to the fact that most of the cheatable zinc is found in the cerebral regions and that very low amount of free zinc is available in the cerebellum of normal mice brain.

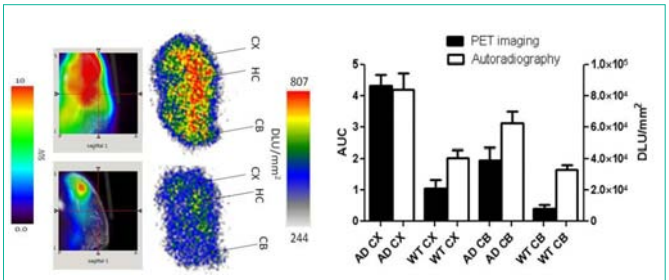

Figure 6: Correlation between PET and autoradiography imaging: Data represent mean AUC of PET images ± SE, and mean digital light unit/mm²± SE in the cortex and the cerebellum of AD and control mice. (WT: Wild Type; CX: Cortex; HC: Hippocampus; CB: Cerebellum; DLU: Digital Light Unit).

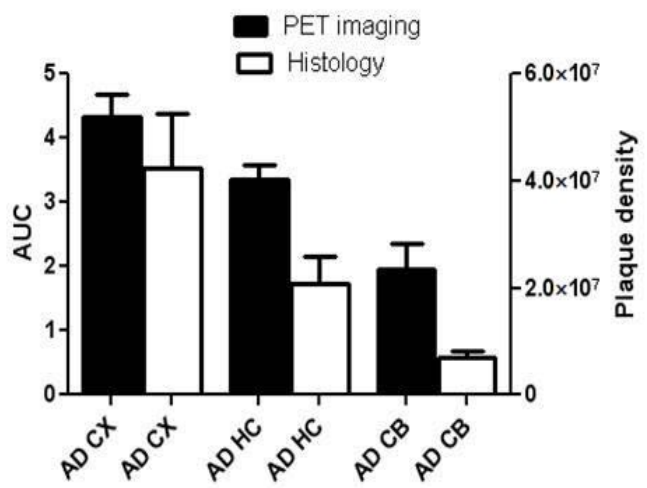

Figure 7: Correlation between histology and PET imaging: Data represent mean AUC of PET images ± SE, and mean plaque density unit/mm²± SE in the cortex (CX), hippocampus (HC) and the cerebellum (CB) of AD mice.

PET ligands based on Congo red and thioflavine derivatives *such as* Pittsburgh Compound B (^{11}C-PiB) have shown the potential for specifically binding amyloid plaques in AD patients with higher retention than that in controls, and a good correlation with FDG PET [48]. Other agents labeled with C-11 are also reported [49]. ^{18}F labeled agents such as ^{18}F-flutemetamol, florbetaben, florbetapir, AZD 4694 are being developed as ^{18}F has longer half-life (110 min vs. 20 min for ^{11}C) and more convenient for production and transportation [50-54]. Neuraceq® (^{18}F-florbetaben) received regulatory approval in Europe and USA last year. It is the third amyloid agent approved for clinical use in the U.S., in addition to Amyvid® (^{18}F-florbetapir) and Vizamyl® (^{18}F-flutemetamol). A positive beta-amyloid scan could signal Alzheimer's disease, whereas a negative scan can rule out the possibility of Alzheimer's. Before amyloid imaging, proof of amyloid burden in the brain was only possible by autopsy. Although PIB and ^{18}F-FDDNP have shown the potential for binding to plaques *in vitro*, they both failed to differentiate between control and AD mice *in vivo* imaging [55]. In the most extensive longitudinal PET study conducted in AD (APP-Swe) mouse model using ^{18}F labeled amyloid tracer, ^{18}F-florbetaben, Rominger et al, [56] demonstrated that first appearance of discernible β-amyloid plaque load at 13 months and a progression to 20 mo.

Conclusions

^{18}F-HOQ has high affinity for Aβ-Zn aggregates. Brain uptake by autoradiography and PET correlated with plaque density. Plaques could be imaged in APP/PS1 Tg mice starting at an early age of 6 months, but could not be imaged in APOE4 mice even at 12 months. Imaging results may depend upon the age of the animals and the animal model used. ^{18}F-HOQ may be useful in monitoring the progression of Aβ plaque deposition in suitable AD animal models by PET imaging and in assessing efficacy of therapeutic agents aimed at reduction of amyloid plaque burden. ^{18}F labeled quinoline derivatives present interesting alternatives to derivatives of amyloid binding dyes

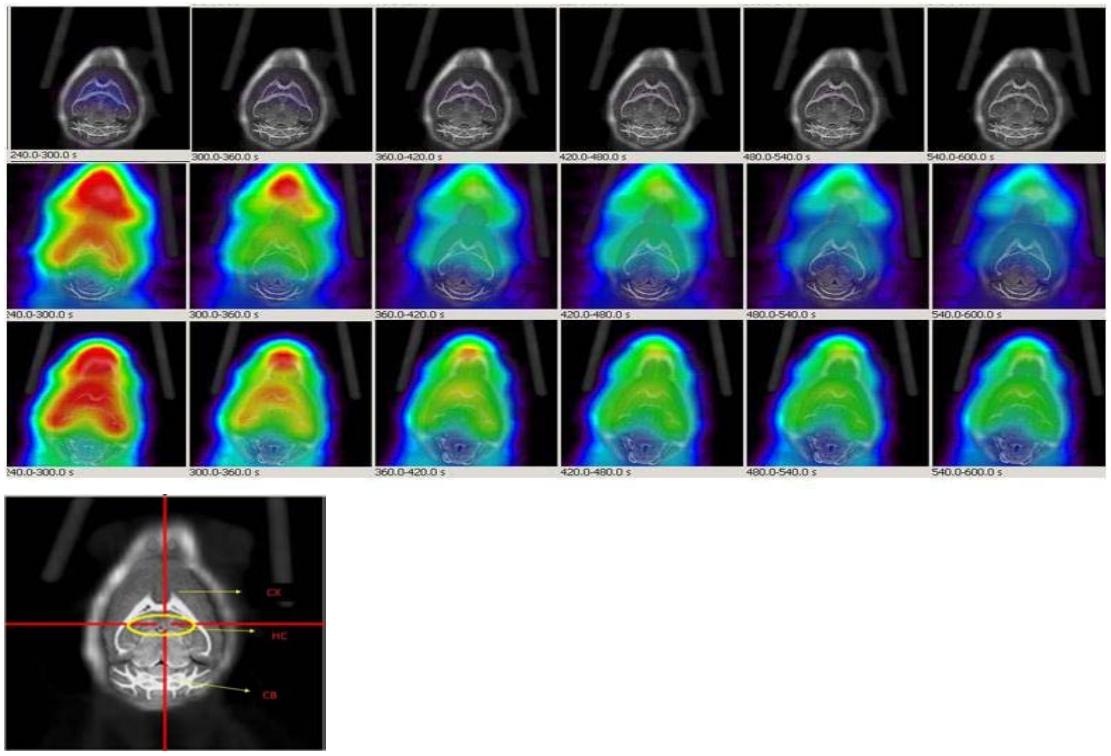

Figure 8: Dynamic PET images (1min/image, 5min-10min) post injection of ^{18}F-HOQ show the differences between brain uptakes of 12 months old control mouse (1st row: 6 images), 6 months old AD mouse (2nd row: 6 images) and 12 months old AD mouse (3rd row: 6 images). The view is coronal section at the level of the hippocampus as indicated in the brain atlas labeled image. Differences in brain uptake could be observed in AD mice as early as 6 months. Lower image represents mouse brain atlas. (CX: Cortex; HC: Hippocampus; CB: Cerebellum).

such as Congo red and thioflavin in imaging Alzheimer's plaques and warrant further investigation.

Acknowledgements

Authors thank the technical support and advice of Patrick Thomas, Anjali Gupta, Michael Long, LakshmanManjunath and Drs. Bao-Xi Qu, Michael Bennett. Thanks to Pam Curry for preparation of figures. Financial support of Worsham Fund and NIH is greatly appreciated. Studies were supported by Worsham Fund and NIH (NIA) Grant# 1RC1AG03308.

References

1. Hebert LE, Scherr PA, Bienias JL, Bennett DA, Evans DA. Alzheimer disease in the US population: prevalence estimates using the 2000 census. Arch Neurol. 2003; 60: 1119-1122.
2. Hardy J, Allsop D. Amyloid deposition as the central event in the aetiology of Alzheimer's disease. Trends Pharmacol Sci. 1991; 12: 383-388.
3. Small SA, Duff K. Linking Abeta and tau in late-onset Alzheimer's disease: a dual pathway hypothesis. Neuron. 2008; 60: 534-542.
4. Hardy JA, Higgins GA. Alzheimer's disease: the amyloid cascade hypothesis. Science. 1992; 256: 184-185.
5. Hardy J, Selkoe DJ. The amyloid hypothesis of Alzheimer's disease: progress and problems on the road to therapeutics. Science. 2002; 297: 353-356.
6. Nordberg A. PET imaging of amyloid in Alzheimer's disease. Lancet Neurol. 2004; 3: 519-527.
7. Henriksen G, Yousefi BH, Drzezga A, Wester HJ. Development and evaluation of compounds for imaging of beta-amyloid plaque by means of positron emission tomography. Eur J Nucl Med Mol Imaging. 2008; 35 Suppl 1: S75-81.
8. Kadir A, Nordberg A. Target-specific PET probes for neurodegenerative disorders related to dementia. J Nucl Med. 2010; 51: 1418-1430.
9. Zhu L, Ploessl K, Kung HF. PET/SPECT imaging agents for neurodegenerative diseases. Chem Soc Rev. 2014; 43: 6683-6691.
10. Frisoni GB. PET and 18F ligands in the diagnosis of Alzheimer's disease. Lancet Neurol. 2011; 10: 397-399.
11. Mathis CA, Mason NS, Lopresti BJ, Klunk WE. Development of positron emission tomography Î²-amyloid plaque imaging agents. Semin Nucl Med. 2012; 42: 423-432.
12. Vlassenko AG, Benzinger TL, Morris JC. PET amyloid-beta imaging in preclinical Alzheimer's disease. Biochim Biophys Acta. 2012; 1822: 370-379.
13. Vallabhajosula S. Positron Emission Tomography Radiopharmaceuticals for Imaging Brain Beta-Amyloid. SeminNucl Med. 2011; 41: 283-299.
14. Barrio JR, Satyamurthy N, Huang SC, Petric A, Small GW, Kepe V. Dissecting molecular mechanisms in the living brain of dementia patients. Acc Chem Res. 2009; 42: 842-850.
15. Klunk WE, Mathis CA. The future of amyloid-beta imaging: a tale of radionuclides and tracer proliferation. Curr Opin Neurol. 2008; 21: 683-687.
16. Någren K, Halldin C, Rinne JO. Radiopharmaceuticals for positron emission tomography investigations of Alzheimer's disease. Eur J Nucl Med Mol Imaging. 2010; 37: 1575-1593.
17. Mathis CA, Wang Y, Holt DP, Huang GF, Debnath ML, Klunk WE. Synthesis and evaluation of 11C-labeled 6-substituted 2-arylbenzothiazoles as amyloid imaging agents. J Med Chem. 2003; 46: 2740-2754.
18. Kung HF, Choi SR, Qu W, Zhang W, Skovronsky D. 18F stilbenes and styrylpyridines for PET imaging of A beta plaques in Alzheimer's disease: a miniperspective. J Med Chem. 2010; 53: 933-941.
19. Brewer GJ. Issues raised involving the copper hypotheses in the causation of Alzheimer's disease. Int J Alzheimers Dis. 2011; 2011: 537528.
20. Brewer GJ. Copper toxicity in Alzheimer's disease: cognitive loss from ingestion of inorganic copper. J Trace Elem Med Biol. 2012; 26: 89-92.
21. Squitti R, Ghidoni R, Scrascia F, Benussi L, Panetta V, Pasqualetti P, et al. Free copper distinguishes mild cognitive impairment subjects from healthy elderly individuals. J Alzheimers Dis. 2011; 23: 239-248.
22. Arnal N, Morel GR, Alaniz MJT, Castillo O, Marra CA. Role of Copper and Cholesterol Association in the Neurodegenerative process. International Journal of Alzheimer's Disease. 2013; 2013: 1-15.
23. Watt NT, Whitehouse IJ, Hooper NM. The Role of Zinc in Alzheimer's Disease. International Journal of Alzheimer's Disease. 2011; 2011: 1-10.
24. Lovell MA, Robertson JD, Teesdale WJ, Campbell JL, Markesbery WR. Copper, iron and zinc in Alzheimer's disease senile plaques. J Neurol Sci. 1998; 158: 47-52.
25. Lee JY, Cole TB, Palmiter RD, Suh SW, Koh JY. Contribution by synaptic zinc to the gender-disparate plaque formation in human Swedish mutant APP transgenic mice. Proc Natl Acad Sci U S A. 2002; 99: 7705-7710.
26. Suh SW, Jensen KB, Jensen MS, Silva DS, Kesslak PJ, Danscher G, et al. Histochemically-reactive zinc in amyloid plaques, angiopathy, and degenerating neurons of Alzheimer's diseased brains. Brain Res. 2000; 852: 274-278.
27. Stoltenberg M, Bush AI, Bach G, Smidt K, Larsen A, Rungby J, et al. Amyloid plaques arise from zinc-enriched cortical layers in APP/PS1 transgenic mice and are paradoxically enlarged with dietary zinc deficiency. Neuroscience. 2007; 150: 357-369.
28. Li-hong Z, Dan YU, Xin W, Wei Z, MingR, Zhan-youW. Distribution of zinc ions and zinc transporter-6 in the APP/PS1 transgenic mouse cerebellum. Fudan University Journal of Medical Sciences. 2009; 36: 65-69.
29. Sekler I, Moran A, Hershfinkel M, Dori A, Margulis A, Birenzweig N, et al. Distribution of the zinc transporter ZnT-1 in comparison with chelatable zinc in the mouse brain. J Comp Neurol. 2002; 447: 201-209.
30. Bush AI. The metallobiology of Alzheimer's disease. Trends Neurosci. 2003; 26: 207-214.
31. Cherny RA, Atwood CS, Xilinas ME, Gray DN, Jones WD, McLean CA, et al. Treatment with a copper-zinc chelator markedly and rapidly inhibits beta-amyloid accumulation in Alzheimer's disease transgenic mice. Neuron. 2001; 30: 665-676.
32. Yassin MS, Ekblom J, Xilinas M, Gottfries CG, Oreland L. Changes in uptake of vitamin B(12) and trace metals in brains of mice treated with clioquinol. J Neurol Sci. 2000; 173: 40-44.
33. Bush AI. Metal complexing agents as therapies for Alzheimer's disease. Neurobiol Aging. 2002; 23: 1031-1038.
34. Bush AI. Drug development based on the metals hypothesis of Alzheimer's disease. J Alzheimers Dis. 2008; 15: 223-240.
35. Cherny RA, Atwood CS, Xilinas ME, Gray DN, Jones WD, McLean CA, et al. Treatment with a copper-zinc chelator markedly and rapidly inhibits beta-amyloid accumulation in Alzheimer's disease transgenic mice. Neuron. 2001; 30: 665-676.
36. Bush AI, Tanzi RE. Therapeutics for Alzheimer's disease based on the metal hypothesis. Neurotherapeutics. 2008; 5: 421-432.
37. Ritchie CW, Bush AI, Mackinnon A, Macfarlane S, Mastwyk M, MacGregor L, et al. Metal-protein attenuation with iodochlorhydroxyquin (clioquinol) targeting Abeta amyloid deposition and toxicity in Alzheimer disease: a pilot phase 2 clinical trial. Arch Neurol. 2003; 60: 1685-1691.
38. Di Vaira M, Bazzicalupi C, Orioli P, Messori L, Bruni B, Zatta P. Clioquinol, a drug for Alzheimer's disease specifically interfering with brain metal metabolism: structural characterization of its zinc(II) and copper(II) complexes. Inorg Chem. 2004; 43: 3795-3797.
39. Opazo C, Luza S, Villemagne VL, Volitakis I, Rowe C, Barnham KJ, et al. Radioiodinated clioquinol as a biomarker for beta-amyloid: Zn complexes in Alzheimer's disease. Aging Cell. 2006; 5: 69-79.

40. Roney CA, Arora V, Kulkarni PV,Antich PP, Bonte FJ. Nanoparticulate Radiolabelled Quinolines Detect Amyloid Plaques in Mouse Models of Alzheimer's Disease. International Journal of Alzheimer's Disease. 2009; 2009: 1-10.

41. Kulkarni PV, Vasdev N, Arora V, Hao G, Long M, Slavine N, et al. PET imaging of Alzheimer's disease (AD) transgenic mice with F–18 labeled hydroxyquinoline derivative. J Nucl Med Meeting abstract 2010; 51:1746.

42. Vasdev N, Cao P, Oosten EM, Wilson AA, Houle S, Hao G, et al. Synthesis and PET imaging studies of [18F]2-fluoroquinolin-8-ol ([18F]CABS13) in transgenic mouse models of Alzheimer's disease. Med. Chem. Commun. 2012; 3: 1228-1230.

43. Selkoe DJ. Alzheimer's disease: genes, proteins, and therapy. Physiol Rev. 2001; 81: 741-766.

44. Fox NW, Johnstone EM, Ward KE, Schrementi J, Little SP. APP gene promoter constructs are preferentially expressed in the CNS and testis of transgenic mice. Biochem Biophys Res Commun. 1997; 240: 759-762.

45. Johnson-Wood K, Lee M, Motter R, Hu K, Gordon G, Barbour R, et al. Amyloid precursor protein processing and A beta42 deposition in a transgenic mouse model of Alzheimer disease. Proc Natl Acad Sci U S A. 1997; 94: 1550-1555.

46. Qu B, Boyer PJ, Johnston SA, Hynan LS, Rosenberg RN. Abeta42 gene vaccination reduces brain amyloid plaque burden in transgenic mice. J Neurol Sci. 2006; 244: 151-158.

47. Slavine NV,McColl RW, Kulkarni PV. 3D Image Processing and Software for Improving the Quantitative Accuracy of PET Image Recovery. Patent disclosure filed with UT Southwestern Medical Center at Dallas in July 26, 2011, UT # 2475

48. Klunk WE, Engler H, Nordberg A, Wang Y, Blomqvist G, Holt DP, et al. Imaging brain amyloid in Alzheimer's disease with Pittsburgh Compound-B. Ann Neurol. 2004; 55: 306-319.

49. Nyberg S, Jönhagen ME, Cselényi Z, Halldin C, Julin P, Olsson H, et al. Detection of amyloid in Alzheimer's disease with positron emission tomography using [11C]AZD2184. Eur J Nucl Med Mol Imaging. 2009; 36: 1859-1863.

50. Rowe CC, Villemagne VL. Brain amyloid imaging. J Nucl Med Technol. 2013; 41: 11-18.

51. Wong DF, Rosenberg PB, Zhou Y, Kumar A, Raymont V, Ravert HT, et al. In vivo imaging of amyloid deposition in Alzheimer disease using the radioligand 18F-AV-45 (florbetapir [corrected] F 18). J Nucl Med. 2010; 51: 913-920.

52. Joshi AD, Pontecorvo MJ, Clark CM, Carpenter AP, Jennings DL, Sadowsky CH, et al. Performance characteristics of amyloid PET with florbetapir F 18 in patients with alzheimer's disease and cognitively normal subjects. J Nucl Med. 2012; 53: 378-384.

53. Barthel H, Gerz HJ, Dresel S, Peters O, Bartenstein P, Buerger K, et al. Cerebral amyloid-? PET with florbetaben (18F) in patients with Alzheimer's disease healthy control: A multicenter phase 2 diagnostic study. Lancet Neurology. 2011; 10: 424-435.

54. Thurfjell L, Lötjönen J, Lundqvist R, Koikkalainen J, Soininen H, Waldemar G, et al. Combination of biomarkers: PET [18F]flutemetamol imaging and structural MRI in dementia and mild cognitive impairment. Neurodegener Dis. 2012; 10: 246-249.

55. Kuntner C, Kesner AL, Bauer M, Kremslehner R, Wanek T, Mandler M, et al. Limitations of small animal PET imaging with [18F]FDDNP and FDG for quantitative studies in a transgenic mouse model of Alzheimer's disease. Mol Imaging Biol. 2009; 11: 236-240.

56. Rominger A, Brendel M, Burgold S, Keppler K, Baumann K, Xiong G, et al. Longitudinal Assessment of Cerebral ?-Amyloid Deposition in Mice Overexpressing Swedish Mutant ?-Amyloid Precursor Protein Using 18F-Florbetaben PET. Journal of Nuclear Medicine. 2013; 54: 1-8.

Austin J Clin Neurol - Volume 2 Issue 8 - 2015
ISSN : 2381-9154 | www.austinpublishinggroup.com

Citation: Kulkarni PV, Alhasan M, Chiguru S, Arora V, Slavine N, Hao G, et al. Early Detection of Amyloid Plaques in Mouse Models of Alzheimer's Disease by PET with ^{18}F-Hydroxy Quinoline. Austin J Clin Neurol 2015;2(8): 1065.